Calibrating LISA Pathfinder raw data into femto-g differential accelerometry

2017 J. Phys.: Conf. Ser. 840 012002

(http://iopscience.iop.org/1742-6596/840/1/012002)

IOP Conf. Series: Journal of Physics: Conf. Series **840** (2017) 012002 doi:10.1088/1742-6596/840/1/012002

Calibrating LISA Pathfinder raw data into femto-g differential accelerometry

Daniele Vetrugno[1] and Nikolaos Karnesis[2] on behalf of the LPF collaboration

[1] Dipartimento di Fisica, University of Trento and Trento Institute for Fundamental Physics and Application / INFN, 38123 Povo, Trento, Italy
[2] Albert-Einstein-Institut, Max-Planck-Institut für Gravitationsphysik und Universität Hannover, 30167 Hannover, Germany

E-mail: daniele.vetrugno@unitn.it, karnesis@aei.mpg.de

Abstract. LISA Pathfinder is an in-flight test of the local sources of acceleration noise in LISA. The acceleration noise level in LISA Pathfinder is measured by the residual differential acceleration Δg between the two test masses once the coupling to the spacecraft motion has been removed. The full process from raw data to Δg passes through a series of calibration experiments and different data elaboration procedure which are thoroughly used during the mission and represent the baseline for any other further investigation.

1. Introduction

LISA Pathfinder[1] (LPF) is an European Space Agency (ESA) satellite launched on December 3, 2015 aiming to test the technological readiness of the local key hardware and software elements for the Laser Interferometer Space Antenna [2] (LISA) detector, the future space-based gravitational wave observatory. LISA is formed by three spacecraft in a triangular quasi-equilateral constellation around the Sun in a heliocentric orbit. Each satellite is separated by about 5×10^6 km from the other two and encloses two Test-Masses (TMs) which must be in principle freely falling. A passing gravitational wave would make then the TMs oscillate perpendicularly to the direction of gravitational wave propagation. However, this effect is a very tiny one, of the order of $h \sim 10^{-21}$ and can be similarly caused by any other non-gravitational spurious force acting on the TMs. To be able to measure gravitational waves it is necessary not only to measure the relative displacement between TMs with the required precision but also to be able to put the TMs in the most quiet possible free-fall. This last requirements for LISA is encoded in the request for the residual acceleration of each TM, g, to have an amplitude spectral density $S_g^{1/2} < 3$ fm s$^{-2}/\sqrt{\text{Hz}}$ at 0.1 mHz, the lowest frequency of its measurement band. The quality of the free fall depends both on the the drag-free control and on the spurious forces that act on the TMs, which are local sources of noise in LISA and hardly testable or measurable on ground. For this reason ESA decided to launch LPF, a technological demostrator of the local sources of noise on LISA. In particular, LPF is one arm of LISA enclosed in one SC, reducing the arm-length from 5×10^6 km to 0.376 m and placing the two TMs in the same spacecraft. The LISA acceleration noise requirement was relaxed for LPF to $S_{\Delta g}^{1/2} < 30$ fm s$^{-2}/\sqrt{\text{Hz}}$ at 1 mHz, where Δg represents the differential residual acceleration between the two TMs. To

properly measure Δg, the full dynamics of the three body system represented by LPF needs to be calibrated and the contribution of the commanded forces of the controllers and the coupling of TMs motion to the spacecraft need to be subtracted.

In Section 2, the equations of motion of LPF are defined and a model for the calibration and the calculation of Δg is introduced. In Section 3, the Δg workflow from raw data to the ultimate estimation of the residual differential acceleration is presented. Finally, in Section 4, some conlusion about the results of Δg calculation are reported.

2. LPF dynamics

LPF is a dynamical system composed by two 46 mm quasi-cubic TMs, and a SC which encloses and protects them from external disturbanses [3]. Each TM is surrounded by an Electrode Housing [4] (EH) whose electrodes both sense the TM position and actuate forces on all the translational and angular degrees of freedom. Each TM plus EH forms the Gravity Reference Sensor (GRS). A three body dynamical system as LPF cannot be stable. Indeed, any static difference of force between the TMs will eventually push them to hit on their housing walls. Three control loops have been implemented in the Drag Free and Attitude Control System (DFACS) on-board software to make LPF dynamics stable. The Drag-free control [5] leaves TM1 freely falling along x and forces the SC to follow it by means of μ-Newton thrusters driven by the interferometer measurement of the distance between SC and TM1, o_1. The electrostatic suspension control forces TM2 to follow TM1 by means of electrostatic actuation[6] which are driven by a second laser interferometer measurement, o_{12}, which measures the relative displacement between the two TMs. Finally, the spacecraft angular degrees of freedom $\{\Phi_{SC}, H_{SC}, \Theta_{SC}\}$ are controlled by the attitude control loop which is fed by the Autonomous Star Tracker (AST) signal in order to make the solar array panel always pointing towards the Sun and the antenna towards the Earth. All the control loops act to maintain the system stable and to reduce as much as possible the noise contribution, in particular on the main measurement axis, the x-axis in Figure 1.

The quality of the free fall is measured by Δg, the differential acceleration noise between the two TMs, given by

$$\Delta g(t) = \ddot{x}_{12}(t) + \omega_2^2 x_{12}(t) + \Delta\omega^2 x_1(t) - A_{sus} F_{cmd,x2}(t) \tag{1}$$

where x_1 is the coordinate of TM1 along the x-axis and $x_{12} = x_2 - x_1$ is the displacement of TM2 with respect to TM1 aong the same axis. $F_{cmd,x2}$ is the commanded force on TM2. ω_2^2 is the stiffness of TM2 and $\Delta\omega^2 = \omega_2^2 - \omega_1^2$ is the differential stiffness which couples the SC motion to the differential acceleration. Finally, A_{sus} is the gain of the electrostatic commanded force on TM2.

The actual application of eq. (1) to the data of the LPF mission requires some manipulation. First of all, what is measured is not the coordinate x but the interferometric read-out signal o. Using the readouts entails that a whole set of possible sensing cross-talk has to be considered, whose the most important is the common mode cross-coupling, where the o_1 signal is leaking into the o_{12} measurement, through a coupling factor δ_{ifo}. Moreover, eq. (1) assumes that, at any given instant, the coordinates, the readouts and the actuation forces are synchronous, which is simply not true. Instead, they acquire a relative delay τ due to the phasemeter measurement process and to DFACS calculation. It means that any applied force $F_{cmd,x2}(t)$ has been in reality calculated at a previous time $(t-\tau)$, and the corrected force to be considered for the equation of Δg is $F_{cmd,x2}(t-\tau)$, where τ is a free parameter. The delayed force can be linearised for small delay values, as $F_{cmd,x2}(t-\tau) \simeq F_{cmd,x2}(t) - \tau\frac{d(F_{cmd,x2}(t))}{dt}$. Then, the model for $\Delta g(t)$ can be written as

$$\Delta g(t) = \ddot{o}_{12}(t) + \omega_2^2 o_{12}(t) + \Delta\omega^2 o_1(t) - A_{sus} F_{cmd,x2}(t) + C_1 \dot{F}_{cmd,x2}(t) + \delta_{\text{ifo}} \ddot{o}_1(t) \tag{2}$$

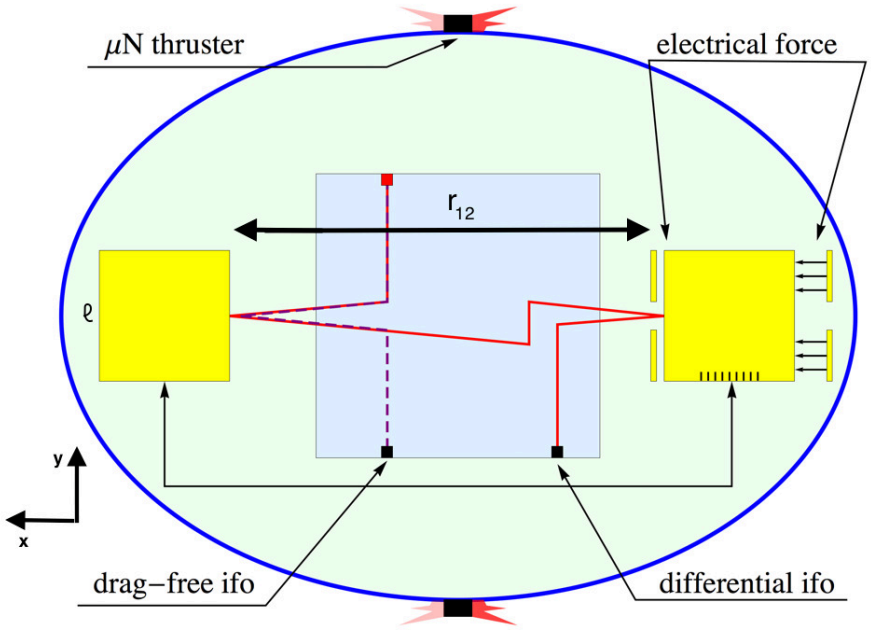

Figure 1: A schematic illustration of LPF. The two TMs in yellow are enclosed by the SC, which is equipped by μNewton thrusters. The TM on the left is called TM1 and is freely falling along the x axis. The drag-free interferometer reads the distance between TM1 and the SC and feeds the μ-Newton thruster to keep the SC centered around TM1. The differential interferometer reads the relative displacements between the TMs and feeds electrodes surrounding the other TM, the TM2, which apply a force on it such to keep the two TMs at a fixed distance.

where $C_1 = \tau A_{sus}$. The values of the free parameters in eq. (2) can be estimated by means of a calibration procedure which consists in exciting the system along the x-axis by injecting fake signals in both the drag-free and electrostatic suspension control loops.

Then, two more additional steps in the calculation of Δg must be considered. The first one is the subtraction of the centrifugal force contribution, Δg_Ω, to Δg at frequencies below 1 mHz. The second one is the subtraction of the high frequencies (> 20 mHz) optical crosstalk. The calibration procedure together with the two additional steps in Δg calculation and the adopted fitting techinque are described in the next section.

3. The Δg workflow

The whole procedure from raw data to the final $\Delta g(t)$ time-series passes through three main steps of data handling, a process that henceforth we can call Δg workflow. The first step requires system calibration via large signal injection, in order to get an estimation of the free parameters of eq. (2) with high precision. With those parameters, a "calibrated" version of the $\Delta g(t)$ time-series can be produced. The second step is then needed to reduce the noise at frequencies below 1 mHz by direct subtraction of the centrifugal forces. Finally, the SC pick-up motion contribution at high frequencies is subtracted.

3.1. System Identification and fitting technique

In order to calibrate the dynamics of LPF described in eq. (2), the system identification experiments must be regularly performed during the duration of the mission, because different working configurations of the system yields different calibration parameters. The system

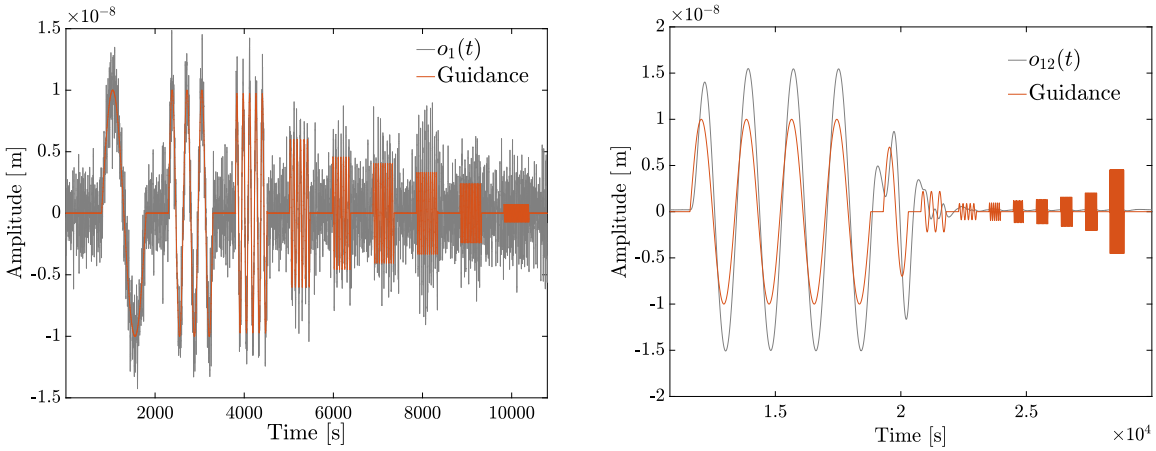

(a) (b)

Figure 2: Batteries of injections during hte system identification experiment. *Left*: Injection sinusoidal signals (red) into the drag-free loop. The response of the system as recorded by the o_1 interferometer is shown in grey. *Right*: The same philosophy applies to the suspension loop as well. The measurement of the o_{12} interferometer is again shown in grey.

identification experiment consists of two trains of guidance injections into the drag-free and the electrostatic suspension loops. The experiment is designed to balance the desire for high signal to noise ration (SNR) for each parameter, and to avoid stimulation of non-linearities of the system. The effect of the guidance injections into o_{12} and o_1 are shown in Figure 2.

The linearised model of eq. (2) allows us to use a Iterative Reweighed Least Square algorithm to fit the data in the frequency domain. The application of this technique to LPF data and its theoretical and empirical justification were firstly introduced in [7]. For each experiment, and in the absence of spurious effects, such as glitches, we were able to subtract all of the induced signal down to comparable levels with the noise runs. The results of the full campaign of system identification experiments will be presented in a future work in prepation.

3.2. Centrifugal force contribution

The Δg time-series calibrated in the previous step and calculated during a pure noise period, that is when no other experiments were running, showed a amplitude spectral density of the residuals noise acceleration exceeding the expected level between $0.1 - 1$ mHz. At those frequencies, the inertial forces associated to SC rotation are expected to contribute to $\Delta g(t)$. Indeed, the attitude control loop driven by the noisy AST, makes the SC rotate. The SC rotation introduces an apparent forces on TMs, that the suspension control tries to compensate in order to keep the TMs at a fixed distance of 0.376 m. Therefore, the commanded force used to calibrate Δg at the previous step contains this contribution which is necessary to subtract from the acceleration noise in eq. (2). A simple calculation shows how this contribution affects Δg and how the relative signal can be obtained.

An observer in a reference system attached to the rotating SC measures an apparent acceleration of one TM due to centrifugal forces along the x-axis given by

$$\ddot{x}(t) = (\vec{\omega} \times (\vec{\omega} \times \vec{r})) \cdot \hat{x}. \tag{3}$$

Assuming the x-axis orientation in Figure 1, the centrifugal acceleration on TM1 and TM2 are respectively

$$\ddot{x_1} = (-\omega_\phi^2 - \omega_\eta^2) x_1 \tag{4}$$

$$\ddot{x_2} = (\omega_\phi^2 + \omega_\eta^2)x_2 \tag{5}$$

where ω_ϕ and ω_η are the SC angular velocities around z and y, respectively. The centrifugal contribution to the differential acceleration between the two TMs is then given by

$$\Delta g_\Omega = \ddot{x_2} - \ddot{x_1} = (\omega_\phi^2 + \omega_\eta^2)(x_2 + x_1) \tag{6}$$

In case of a perfect centering between TMs and spacecraft, $(x_2 + x_1) = 2x_1 = 2x_2 = 0.376$ m, the distance between the two TMs. This would reduce the acceleration due to centrifugal forces to

$$\Delta g_\Omega = (\omega_\phi^2 + \omega_\eta^2)2x_1. \tag{7}$$

If ω_ϕ and ω_η were measurable parameters, the term in eq. (7) can be subtracted directly from Δg in eq. (2).

However, the SC angular velocity is not directly available in LPF telemetry. But we are able to synthesise it by combining the Autonoumous Star Tracker signal in the form of quaternions with the mean applied torques on the TMs. But even if the quaternions are directly linked to the SC angular velocity, they are very noisy between $0.1 - 1$ mHz and cannot be used directly. A polynomial fit to the equivalent angular velocity extracted from the quaternions allows to calculate the DC angular velocity of the spacecraft, ω_{DC}. Then, by integrating the commanded torques on the TMs, which are the driving signal to the attitude control loop which in turn makes the SC rotate, the in-band angular velocity, ω_{noise}, can be calculated. The final SC angular velocity for each angular degree of freedom can be calculated as $\omega = \omega_{DC} + \omega_{noise}$ and the relative contribution of the centrifugal forces, Δg_Ω subtracted from $\Delta g(t)$.

3.3. SC pick-up motion subtraction

In [8] it was shown that in the frequency band between 200 mHz - 20 mHz the pick-up of the SC motion leaking into the main differential measurement can be detected. In order to measure this contribution a fit to the following linear model has been performed

$$\Delta g_{x-talk} = C_1\ddot{\overline{\phi}}[t] + C_2\ddot{\overline{\eta}}[t] + C_3\ddot{\overline{y}}[t] + C_4\ddot{\overline{z}}[t] + C_5\overline{y}[t] + C_6\overline{z}[t] + \delta_{\text{ifo}}\ddot{o}_1[t], \tag{8}$$

where each $k \in \{\phi, \eta, y, z\}$ is a different coordinate, and the $\bar{k}$ denotes the mean displacement or rotation of both test-masses along the coordinate k, or equivalently SC motion along $-k$. The δ_{ifo} term refers to signal leakage from o_1 to the o_{12} readout. The model of eq. (8) performs really well, subtracting the excess bulge-signal down to the white noise levels of the interferometer readout noise. As expected the parameter estimates depend on the geometrical configuration of the three-body system. However, different combinations of signals can yield very similar and satisfactory results, and that means that the model provides no direct physical interpretation of the coefficients C_i. More information on the given cross-talk model, as well as for an alternative approach to suppress the cross coupling by realigning the test masses, is given in Wanner *et al* in the same proceedings.

4. Conclusions

In this paper, the main steps of the Δg workflow were presented and the full post-processing procedure to get the final product of the noise acceleration Δg is described. This procedure has been routinely performed during the whole mission and has been adopted as the baseline for any other investigation and results, such as those presented for the first time in [8]. The robustness and reliability of the whole Δg workflow has been scrupulously tested and the results of these tests will be presented in following papers which are right now in preparation.

References

[1] P. McNamara, S. Vitale, and K. Danzmann, *Classical Quantum Gravity* **25** (2008) 114034.
[2] K. Danzmann et al., *LISA: Unveiling a Hidden Universe Report* No. ESA/SRE2011(2011)3.
[3] S. Anza et al., *Classical Quantum Gravity* **22** (2005) S125.
[4] R. Dolesi et al., *Classical Quantum Gravity* **20** (2003) S99.
[5] W. Fichter, P. Gath, S. Vitale, and D. Bortoluzzi, *Classical Quantum Gravity* **22** (2005) S139.
[6] F Antonucci et al., *Classical Quantum Gravity* **28** (2011) 094002.
[7] S. Vitale et al.,*Phys. Rev. D* **90** (2014) 042003 .
[8] M. Armano et al. *Phys. Rev. Lett.* **116** (2016) 231101.